A Characteristic-Based Domain Decomposition and Space-Time Local Refinement Method for Advection-Reaction Equations with Interfaces

HONG WANG [1], JAN E. VÅG [2], and MAGNE S. ESPEDAL [2]

Abstract

In this paper we present a characteristic-based, noniterative, nonoverlapping, domain decomposition and space-time local refinement method to solve the initial-boundary value problems for advection-reaction equations with various interfaces.

1 Introduction

Advection-reaction partial differential equations arise in a variety of applications and often cause numerical difficulties. Conventional space-centered finite difference/element methods usually result in severe non-physical oscillatory solutions. While upstream weighting techniques can eliminate the oscillations, they generate numeri-

[1] Department of Mathematics, University of South Carolina, Columbia, SC 29208, USA
[2] Department of Mathematics, University of Bergen, Alleg. 55, 5007, Bergen, Norway

Domain Decomposition Methods in Sciences and Engineering, edited by R. Glowinski *et al.*

cal solutions with serious numerical dispersion [EW83]. Moreover, practical problems often have various physical and numerical interfaces that introduce further complexities. Physical interfaces arise when the media properties change abruptly, leading to advection-reaction equations with discontinuous coefficients. Numerical interfaces arise when domain decomposition or local refinement techniques are used. The solutions of advection-reaction equations are generally smooth outside some small regions and may have sharp fronts/discontinuity inside, which need to be resolved accurately free of oscillation or numerical dispersion in practice. In this case local refinement should be used within the sharp front regions. Domain decomposition should be used when the governing equations (especially in the case of strongly coupled systems) are imposed over large domains. One can see that numerical interfaces are introduced in either case.

It is more difficult to develop domain decomposition and local refinement techniques for advection-reaction equations than it is for elliptic and parabolic equations, because in the context of advection-reaction equations locally generated numerical errors at the boundaries/interfaces can be propagated into the domain and destroy the overall accuracy/stability of the method. In this paper we present a characteristic-based, noniterative, nonoverlapping, domain decomposition and space-time local refinement method for advection-reaction equations with various physical/numerical interfaces. To demonstrate the ideas, we consider the model problem

$$\begin{aligned} u_t + (V(x,t)\ u)_x + K(x,t)u &= f(x,t), && x \in (a,b),\ t \in (0,T], \\ u(a,t) &= g(t), && t \in (0,T], \\ u(x,0) &= u_0(x), && x \in [a,b]. \end{aligned} \tag{1}$$

Here $V(x,t) > 0$ is a velocity field, $K(x,t)$ is a first-order reaction coefficient, $u_x = \frac{\partial u}{\partial x}$, $u_t = \frac{\partial u}{\partial t}$. $V(x,t)$ is continuously differentiable except at the interfaces d_l ($l = 1, 2, \dots, L-1$ with $a = d_0 < d_1 < \dots < d_{L-1} < d_L = b$) where $V(x,t)$ has a jump discontinuity in x. Problem (1) is closed by the following interface conditions

$$V(d_l-,t)u(d_l-,t) = V(d_l+,t)u(d_l+,t), \quad t \in [0,T],\ l = 1, 2, \dots, L-1. \tag{2}$$

2 An ELLAM Scheme

In this section we present an ELLAM (Eulerian-Lagrangian localized adjoint method) scheme for problem (1) with smooth coefficients. Based on this scheme we develop a domain decomposition and local refinement method. ELLAM was originally developed for the solution of advection-diffusion equations with general boundary conditions [CRHE90]. Let I and N be two positive integers, define the spatial and temporal partitions $x_i = a + i\Delta x$ for $i = 0, 1, \dots, I$ and $t_n = n\Delta t$ for $n = 0, 1, \dots, N$ with $\Delta x = (b-a)/I$ and $\Delta t = T/N$. In addition, we introduce a local time refinement $t_{n.i}$ at the outflow boundary $\{b\} \times [t_n, t_{n+1}]$ by $t_{n+1} = t_{n.I} > t_{n.I+1} > \dots > t_{n.I+IC} > t_{n.I+IC+1} = t_n$, whose exact definition will be given in Section 4. At time t_{n+1} (or the outflow boundary $x = b$), we define an approximate characteristic $X(\theta; x, t_{n+1})$, $\theta \in [t_n, t_{n+1}]$, (or $X(\theta; b, t)$, $\theta \in [t_n, t]$,) to be the tangent line emanating backward from (x, t_{n+1}) (or (b, t)). We also let $x^* = X(t_n; x, t_{n+1})$, $b^*(t) = X(t_n; b, t)$, and $\tilde{a}$ to satisfy $a = X(t_n; \tilde{a}, t_{n+1})$.

With any space-time test functions w that vanish outside of $[a, b] \times (t_n, t_{n+1}]$ and are discontinuous in time at time t_n, one can write a space-time variational formulation for the governing equation in (1) as follows

$$\begin{aligned} &(u_{n+1}, w_{n+1})_{L^2(a,b)} + < [Vu]_c, w_c > |_{c=a}^{c=b} - < (u, [w_t + Vw_x - Kw]) > \\ &= (u_n, w_n^+)_{L^2(a,b)} + < (f, w) >, \end{aligned} \tag{3}$$

where $(u_n, w_n)_{L^2(a,b)} = \int_a^b u(x, t_n) w(x, t_n) dx$, $< u_c, w_c >= \int_{t_n}^{t_{n+1}} u(c, t) w(c, t) dt$ for $c = a$ or b, $< (u, w) >=< (u, w)_{L^2(a,b)} >$, and $w_n^+ = \lim_{t \to t_n, t > t_n} w(x, t)$.

It is difficult to find the test functions w to satisfy $w_t + Vw_x - Kw = 0$ since one cannot track the characteristics exactly, in general. Nevertheless, the test functions w_i, which are defined by $w_i(X(\theta; x, t_{n+1}), \theta) = w_i(x, t_{n+1}) e^{-K(x, t_{n+1})(t_{n+1} - \theta)}$ for $\theta \in [t_n, t_{n+1}]$ and $i = 0, 1, \ldots, I$, and by $w_i(X(\theta; b, t), \theta) = w_i(b, t) e^{-K(b,t)(t-\theta)}$ for $\theta \in [t_n, t]$ and $i = I, I+1, \ldots, I + IC + 1$, satisfy $w_t + Vw_x - Kw = 0$ approximately. Substituting w_i for w in (3), one can rewrite (3) as follows

$$\begin{aligned} &(u_{n+1}, w_{n+1})_{L^2(a,b)} + < V_b u_b, w_b > - < (u, [w_t + Vw_x - Kw]) > \\ &= (\Psi_{n+1}^{(1)} u_n^*, w_{n+1})_{L^2(\tilde{a},b)} + < \Psi_b^{(2)} u_n^*, w_b > + (\Psi_{n+1}^{(3)} f_{n+1}, w_{n+1})_{L^2(a,b)} \\ &+ < \Psi_b^{(4)} f_b, w_b > + < V_a g, w_a > + R(f, w). \end{aligned} \tag{4}$$

Here $u_n^* = u(x^*, t_n)$ in $(\cdot, \cdot)$ with $x^* = X(t_n; x, t_{n+1})$ and $u_n^* = u(b^*(t), t_n)$ in $< \cdot, \cdot >$ with $b^*(t) = X(t_n; b, t)$. $R(f, w)$ is a truncation-error term resulting from the application of the backward Euler quadrature to the last term on the right-hand side of Equation (4). $\Psi_{n+1}^{(1)} = 1 + O(\Delta t)$, $\Psi_b^{(2)} = V(b, t)(1 + O(\Delta t))$, $\Psi_{n+1}^{(3)} = \Delta t(1 + O(\Delta t))$, $\Psi_b^{(4)} = \Delta t(1 + O(\Delta t))$ are Jacobian-related factors whose exact forms are omitted here.

In the numerical scheme the trial functions U are chosen to be piecewise-linear functions at the time t_{n+1} and at the outflow boundary. Note that $w_{it} + Vw_{ix} - Kw = 0$ approximately, the term $< (u, [w_t + Vw_x - Kw]) >$ should be small and dropping it introduces negligible errors. Replacing u by U in (4) and dropping the last terms on both the left-hand and right-hand sides of Equation (4), one obtains an ELLAM scheme at $i = 1, 2, \ldots, I + IC$ as follows

$$\begin{aligned}&(U_{n+1}, \hat{w}_{i,n+1})_{L^2(a,b)} + < V_b U_b, \hat{w}_{ib} > \\ &= (\Psi^{(1)}_{n+1} U^*_n, \hat{w}_{i,n+1})_{L^2(\tilde{a},b)} + < \Psi^{(2)}_b U^*_n, \hat{w}_{ib} > + (\Psi^{(3)}_{n+1} f_{n+1}, \hat{w}_{i,n+1})_{L^2(a,b)} \\ &+ < \Psi^{(4)}_b f_b, \hat{w}_{ib} > + < V_a g, \hat{w}_{ia} >,\end{aligned} \tag{5}$$

where $\hat{w}_i = w_i$ for $i = 1, 2, \ldots, I + IC - 1$, $\hat{w}_1 = w_0 + w_1$, $\hat{w}_{I+IC} = w_{I+IC} + w_{I+IC+1}$. Since $U(a, t_{n+1}) = g(t_{n+1})$ is known, no equation is needed at $i = 0$. Thus, for $i = 1$ in Equation (5) we use $\hat{w}_1 = w_1 + w_0$ instead of w_1 on $[a, x_1]$. Similarly, because $U(b, t_n)$ is known from the computations at the previous time t_n, we choose $\hat{w}_{I+IC}$ instead of w_{I+IC} on $[t_n, t_{n+1,I+IC}]$ in Equation (5) for $i = I + IC$.

With the given boundary condition at the inflow boundary $x = a$ and the known solution at the time t_n, one can solve Equation (5) for the ELLAM approximation U at the time t_{n+1} and at the outflow boundary $x = b$. The scheme has a well-conditioned, symmetric and positive definite (tridiagonal in one dimension) coefficient matrix without any artificial boundary conditions added.

3 A Space-Time Local Refinement and Domain Decomposition Algorithm

Based on the scheme (5) we present a noniterative, nonoverlapping, domain decomposition and space-time local refinement method for problem (1) with interfaces at d_l $(l = 1, 2, \ldots, L - 1)$: Partition the time interval $[0, T]$ into K intervals $[T_{k-1}, T_k]$ with $0 = T_0 < T_1 < \ldots < T_{k-1} < T_k = T$.

(1) With the given initial and boundary conditions in (1), apply Equation (5) to solve problem (1) over the space-time domain $[a, d_1] \times [0, T_1]$. The solution $U(x, t)$ over this domain defines the left-limit $U(d_1-, t)$ for $t \in [0, T_1]$ and $U(x, T_1)$ for $x \in [a, d_1]$.

(2) When $V(x, t)$ is discontinuous at $x = d_1$, U is discontinuous at the same location too. The continuity condition (2) yields the right-limit $U(d_1+, t)$ for $t \in [0, T_1]$. With $U(d_1+, t)$ as the inflow boundary condition and the initial condition in (1), one applies Equation (5) to solve problem (1) over the domain $[d_1, d_2] \times [0, T_1]$, except that the $g(t)$ in the last term on the right-hand side of (5) should be replaced by $U(d_1+, t)$.

(3) With $U(x, T_1)$ $x \in [a, d_1]$ as the initial condition and the inflow boundary condition in (1), apply Equation (5) to solve problem (1) over $[a, d_1] \times [T_1, T_2]$.

(4) Next one applies Equation (5) to solve problem (1) over $[a, d_1] \times [T_2, T_3]$, $[d_1, d_2] \times [T_1, T_2]$, and $[d_2, d_3] \times [T_0, T_1]$. Repeating this process one can obtain the solution $U(x, t)$ over the global domain $[a, b] \times [0, T]$.

It is easy to see that steps 2 and 3 can be performed in parallel. In general, one can solve problem (1) over $[a, d_1] \times [T_{k-1}, T_k]$, $[d_1, d_2] \times [T_{k-2}, T_{k-1}]$, ..., $[d_{k-1}, d_k] \times [T_0, T_1]$, in parallel. Thus, this algorithm actually defines a characteristic-based, noniterative, nonoverlapping, parallelized, domain decomposition algorithm. Secondly, note that this algorithm is well-defined independent of the space-time grids defined on each subdomain $[d_{l-1}, d_l] \times [T_{k-1}, T_k]$. When the solution has a sharp front within $[d_{l-1}, d_l] \times [T_{k-1}, T_k]$ and is smooth outside, one can use refined space-time grids only within this subdomain and coarse grids outside. Thus, this algorithm also gives a space-time local refinement method, which can resolve the sharp front accurately with reasonable computational cost.

4 Conforming/Nonconforming Matching of Interfacial Nodes

In this section we briefly discuss the matching of interfacial nodes. At the current time slab $[d_{l-1}, d_l] \times [t_n, t_{n+1}]$, the following three different partitions of interfaces can be used:

PARTITION 1: One can partition the interface $\{d_l\} \times [t_n, t_{n+1}]$ based on the magnitude of the Courant number $Cu_b = V_b \Delta t / \Delta x$ with $V_b = \max_{t \in [t_n, t_{n+1}]} V(b, t)$. In this case one defines the nodes $t_{n,i} \equiv t_{n+1} - (i - I)\Delta t / Cu_b = t_{n+1} - (i - I)\Delta x / V_b$ for $i = I, I+1, \ldots, I + IC$ and $t_{n,I+IC+1} = t_n$, where IC is the integer part of Cu_b if Cu_b is not an integer and $IC = Cu_b - 1$ otherwise [CRHE90].

PARTITION 2: One can define a uniform partition at the interface $\{d_l\} \times [t_n, t_{n+1}]$ based on the Courant number Cu_b, which is essentially the same as Partition 1.

Notice that partition 1 or 2 defines $U(d_l-, t)$ $(t \in [t_n, t_{n+1}])$ to be a piecewise-linear function on the nodes $t_n = t_{n,I+IC+1} < t_{n,I+IC} < \ldots < t_{n,I+1} < t_{n,I} = t_{n+1}$. On the other hand, the last term on the right-hand side of (5) actually defines the integral of $U(d_l+, t)\hat{w}_i$ on the interval $[t^*_{n,i+1}, t^*_{n,i-1}]$ where $t^*_{n,i}$ is given by $a = X(t^*_{n,i}; x_i, t_{n+1})$ for $i = 0, 1, \ldots, IC_a$ and $t^*_{n,IC_a+1} = t_n$ with IC_a being the integer part of $(\tilde{a} - a)/\Delta x$. In other words, $t^*_{n,i}$ $(i = 0, 1, \ldots, IC_a)$ is the time such that the approximate characteristic extending backward from x_i at time t^{n+1} meets the inflow boundary $x = a$ at $t^*_{n,i}$. Since the $t^*_{n,i}$ $(i = 0, 1, \ldots, IC_a)$ at the interface $\{d_l\} \times [t_n, t_{n+1}]$ are different from $t_{n,i}$ $(i = I, I+1, \ldots, I + IC)$, in general, one has to interpolate $U(d_l-, t)$ on a shifted grid $t_n = t^*_{n,IC+1} < t^*_{n,IC} < \cdots < t^*_{n,1} < t^*_{n,0} = t_{n+1}$ when one used Equation (5) to solve problem (1) on $[d_l, d_{l+1}] \times [t_n, t_{n+1}]$. Thus, Partition 1 or 2 defines a nonconforming matching.

PARTITION 3: We define the nodes $t_{n,I+i}$ from the subdomain $[d_l, d_{l+1}] \times [t_n, t_{n+1}]$ to be equal to $t^*_{n,i}$ from the subdomain $[d_{l-1}, d_l] \times [t_n, t_{n+1}]$. When we use Equation (5) to solve problem (1) over $[d_{l-1}, d_l] \times [t_n, t_{n+1}]$, we obtain $U(d_l-, t)$ defined on the grid $t_n = t^*_{n,IC+1} < t^*_{n,IC} < \cdots < t^*_{n,1} < t^*_{n,0} = t_{n+1}$, which is the same grids over which we need to compute the last integral on the right-hand side of (5). Thus, this partition gives a conforming matching.

5 Numerical Example

In this section we apply Equation (5) to solve problem (1) with discontinuous coefficients. The data are given as follows: the domain $D_1 = (-1, 0)$ and $D_2 = (0, 1)$, the velocity $V_1(x) = 2$ on D_1 and $V_2(x) = 1$ on D_2, $g(t) = 0.0$, the initial condition $u_0(x) = 1000(x + 0.15)^4(x + 0.85)^4$ for $x \in (-0.85, -0.15)$ and 0 otherwise.

Because of the discontinuity of $V(x, t)$ at $x = 0$, the interface condition (2) now reduces to $2u(0-, t) = u(0+, t)$ for $t \in [0, T]$. It is easy to see that the analytical solution of this problem is given by $u(x, t) = u_0(x - 2t)$ for $x \in (-1, 0)$ and $u(x, t) = 2u_0(2(x-t))$ for $x \in (0, 1)$. In Figures 1–2 the numerical solutions are plotted against the analytical ones for time $t = 0.1$, 0.25 and 0.8, respectively. In Figure 1 we used coarser grids on D_1 and finer grids on D_2. The Courant number is 8. One can see that the numerical solutions have been quite accurate. Similar conclusions can be drawn in Figure 2. Our other experiments, which are omitted here, show that when the time step Δt is relatively large, Partition 3 produces a slightly better solution than Partitions 1 and 2 (about 20 % less errors). On the other hand, Partitions 1 and 2 are more feasible and convenient to implement especially for nonlinear problems or multi-dimensional problems.

Acknowledgments

This research was funded in part by DOE DE-ACO5-840R21400, Martin Marietta, Subcontract SK965C and SK966V, by ONR N00014-94-1-1163, by NSF DMS-8922865, by VISTA, a research cooperation between Statoil and the Norwegian Academy of Science and Letters, and by the Norwegian Research Council.

References

[CRHE90] Celia M., Russell T., Herrera I., and Ewing R. (1990) An Eulerian-Lagrangian localized adjoint method for the advection-diffusion equation. *Advances in Water Resources* 13: 187–206.

[EW83] Ewing R.E. (ed.): The Mathematics of Reservoir Simulation. Frontiers in Applied Mathematics, Vol. 1. SIAM, Philadelphia, 1983.

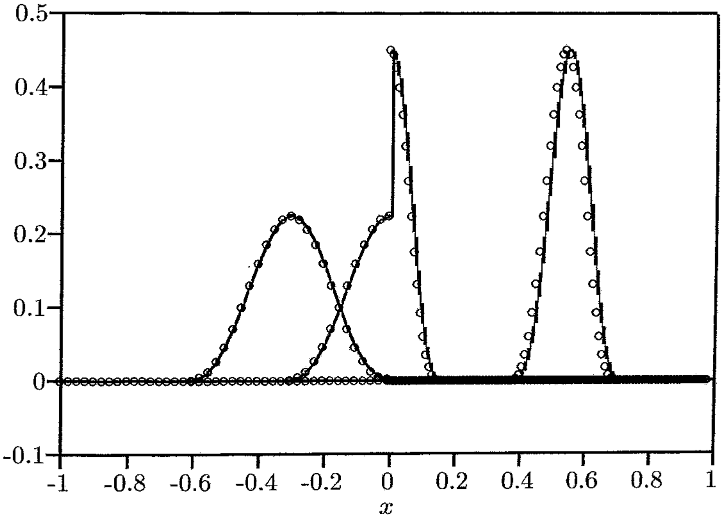

Figure 1 $\Delta t = 0.1$, $\Delta x_1 = 1/40$, $\Delta x_2 = 1/100$, Partition 3 used.

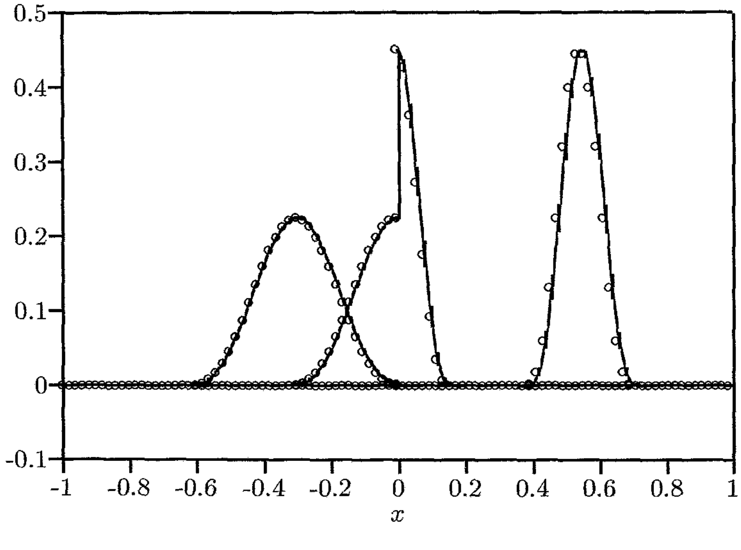

Figure 2 $\Delta t = 0.05$, $\Delta x_1 = 1/50$, $\Delta x_2 = 1/50$, Partition 1 used.